Actinide-Boosting *r* Process in Black-Hole–Neutron-Star Merger Ejecta

Shinya Wanajo,[1,2,*] Sho Fujibayashi,[3,2,1] Kota Hayashi,[1,4] Kenta Kiuchi,[1,4]
Yuichiro Sekiguchi,[4,5] and Masaru Shibata[1,4]

[1]*Max-Planck-Institut für Gravitationsphysik (Albert-Einstein-Institut), Am Mühlenberg 1, D-14476 Potsdam-Golm, Germany*
[2]*Astronomical Institute, Graduate School of Science, Tohoku University, Sendai 980-8578, Japan*
[3]*Frontier Research Institute for Interdisciplinary Sciences, Tohoku University, Sendai 980-8578, Japan*
[4]*Center for Gravitational Physics and Quantum Information, Yukawa Institute for Theoretical Physics,*
Kyoto University, Kyoto 606-8502, Japan
[5]*Department of Physics, Toho University, Funabashi, Chiba 274-8510, Japan*

We examine nucleosynthesis in the ejecta of black-hole–neutron-star mergers based on the results of long-term neutrino-radiation-magnetohydrodynamics simulations for the first time. We find that the combination of dynamical and postmerger ejecta reproduces a solarlike *r*-process pattern. Moreover, the enhancement level of actinides is highly sensitive to the distribution of both the electron fraction and the velocity of the dynamical ejecta. Our result implies that the mean electron fraction of dynamical ejecta should be $\gtrsim 0.05$ in order to reconcile the nucleosynthetic abundances with those in *r*-process-enhanced, actinide-boost stars. Since the tidal ejecta preserve the neutron richness in the inner crust of premerging neutron stars, this result provides an important constraint for nuclear equations of state if black-hole–neutron-star mergers are responsible for actinide-boost stars.

Introduction—One of the long-standing issues in nuclear astrophysics is to determine the mechanism that ensures a robust solarlike *r*-process pattern found in *r*-process-enhanced metal-poor stars (e.g., Ref. [1]). Recent work [2] based on long-term neutrino-radiation-hydrodynamics simulations of neutron-star merger remnants suggests that a combination of dynamical and postmerger ejecta leads to a solarlike *r*-process pattern (see also [3–5], including cases of black-hole–neutron-star mergers). However, these nucleosynthesis studies are not fully self-consistent such that the three-dimensional simulations for the dynamical phase have been followed by axisymmetric simulations with parametrized viscosity effects for the postmerger phase.

Another salient feature observed in *r*-process-enhanced stars is the presence of stars with an excess of the radioactive species Th with respect to a stable element, e.g., Eu. This excess is known as the "actinide boost" [6–9]. The Th/Eu ratio ranges over a factor of 8, $0.14 \leq$ Th/Eu ≤ 1.1 [10,11]. Among those, about one-third of *r*-process-enhanced stars are classified as actinide-boost stars with

Th/Eu > 0.5 (the production ratio of Th/Eu > 0.9 assuming a stellar age of 13 Gyr). The study of nucleosynthesis [12] using a single thermodynamic trajectory has demonstrated that actinides are overproduced if the initial neutron richness is sufficient for fission recycling. However, these studies assumed an equal split of fissioning nuclei, which could result in a significant underestimation of Eu production and thus an overestimation of Th/Eu (see the Supplemental Material [13]).

In this Letter, we present the first nucleosynthesis study based on self-consistent, long-term neutrino-radiation-magnetohydrodynamics simulations in Refs. [31,32]. The aim of this Letter is twofold. One is to examine if black-hole–neutron-star mergers can reproduce solarlike *r*-process patterns as can be seen in *r*-process-enhanced stars. This is important because of the recent observation of gravitational waves from two compact binary coalescences exhibiting properties consistent with black-hole–neutron-star mergers [14]. Second, we attempt to explore the conditions in which actinide boost is realized. Based on our results, we also provide a constraint for nuclear equations of state.

Models—We adopt the results of neutrino-radiation-magnetohydrodynamics simulations of black-hole–neutron-star mergers in Refs. [31,32]. In their models, the temperature-dependent, tabulated nuclear equations of state DD2 [33] or SFHo [34] were adopted, and early dynamical and late postmerger mass ejections were self-consistently computed in a single three-dimensional computational
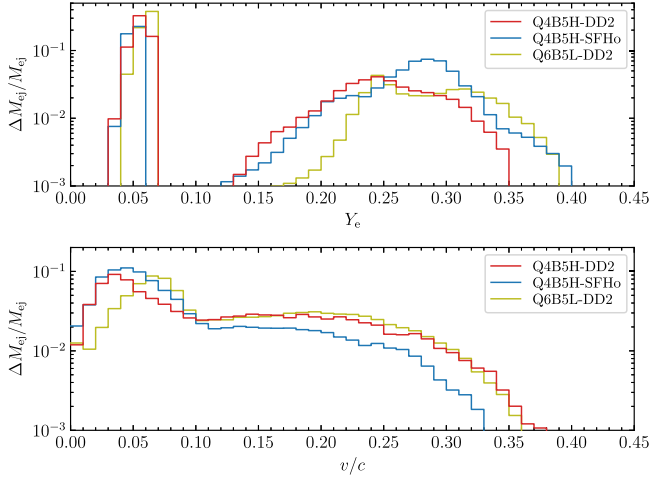
FIG. 1. Mass histograms at the end of simulations with respect to the total ejecta masses for Y_e (top) with an interval of $\Delta Y_e = 0.01$, and v/c (bottom) with an interval of $\Delta(v/c) = 0.01$.
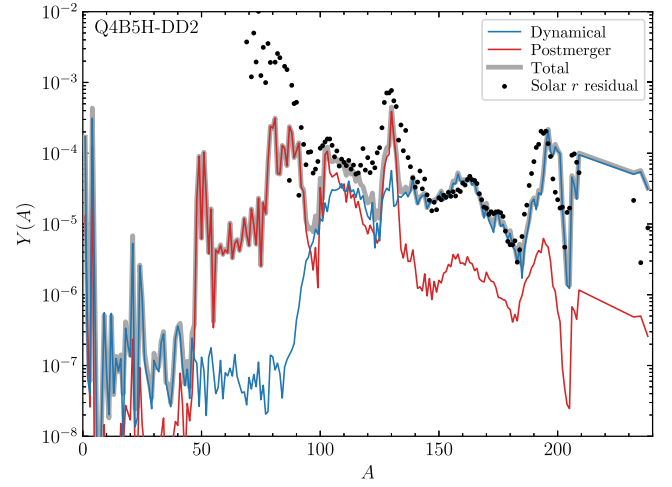

FIG. 2. Total isobaric abundances (gray) as well as those from dynamical (blue) and postmerger (red) ejecta components at the end of simulation (1 yr; all trans-Pb nuclei except for Th and U are assumed to have decayed) for Q4B5H-DD2. The black circles denote the solar r residuals vertically shifted to match the calculated total abundance of ^{153}Eu.

domain. The postmerger mass ejection is predominantly due to the effective viscosity induced by magnetohydrodynamic turbulence.

In this Letter, we take their models of Q4B5H with DD2 and SFHo (hereafter referred to as Q4B5H-DD2 and Q4B5H-SFHo) and Q6B5L with DD2 (Q6B5L-DD2). Here, Q4 and Q6, B5, and H and L stand for the ratios of black-hole masses ($5.4M_\odot$ and $8.1M_\odot$) with respect to that of a neutron star ($1.35M_\odot$), the initial maximum magnetic-field strength (5×10^{16} G), and the grid spacing for the finest refinement level (270 and 400 m), respectively. The ejecta masses were approximately saturated for all models at the end of simulations ($\gtrsim$1–2 s). The total ejecta masses are $M_{\rm ej}/M_\odot = 0.070$, 0.031, and 0.067 for Q4B5H-DD2, Q4B5H-SFHo, and Q6B5L-DD2, respectively.

For nucleosynthesis calculations during postprocessing, about 1400 (of which 400 are for the dynamical component) tracer particles are generated for each model as in Ref. [2]. The method of nucleosynthesis calculations is described in the Supplemental Material [13] (see also Refs. [15–23] therein). Each nucleosynthesis calculation ends at 1 yr. Figure 1 displays the mass histograms for electron fraction (proton number per nucleon) Y_e and velocity v with respect to the speed of light c (bottom). We find both narrow and broad distributions for each model at $Y_e \sim 0.05$–0.06 and 0.1–0.4 originating from dynamical and postmerger ejecta, respectively. The masses of the dynamical ejecta (defined as those with $Y_e < 0.08$) are $M_{\rm ej}/M_\odot = 0.039$ (56% of the total ejecta mass), 0.012 (39%), and 0.046 (69%) for Q4B5H-DD2, Q4B5H-SFHo, and Q6B5L-DD2, respectively. We also find narrow and broad distributions at $v/c \sim 0.03$–0.07 and 0.1–0.4, which come from postmerger and dynamical ejecta, respectively.

r-process abundance patterns—The nucleosynthesis result for model Q4B5H-DD2 is presented in Fig. 2. We find that the dynamical and postmerger ejecta are responsible for the heavy ($A > 130$) and light ($A < 130$) components of r-process abundances, respectively. The ensemble of both components is in good agreement with the pattern of r-process residuals to the solar abundances (r residuals hereafter) [35] for $A \approx 90$–210 (for the comparison with previous studies [3,5], see the Supplemental Material [13]).

In the dynamical ejecta, the abundance pattern for $A < 170$ is determined predominantly by the asymmetric fission from nuclei with $A \sim 260$–280 after the end of an r process. This leads to the diminished second peak ($A \sim 130$) as well as the formation of the silver ($A \sim 100$–110) [24] and rare-earth ($A \sim 160$) [25] peaks. It is important to note that the fission properties in the neutron-rich region, including fission fragment distributions, are currently very uncertain [26–28]. However, we regard the adopted GEF fragment distributions [20] as a reasonable choice for the purposes in this Letter, in which robustly reproducing a solarlike r-process pattern for lanthanides, including Eu, is particularly important (for the comparison with the different predictions of fission fragment distributions, see Supplemental Material [13] and Ref. [29] therein).

Figure 3 compares the elemental abundances normalized by those of Eu for all models. It is noteworthy that the abundance patterns of all models are similar for $40 < Z < 82$ ($90 < A < 206$), which are in good agreement with that of the solar r residuals (although the second peak elements are underproduced). Changing the binary mass ratio (Q6B5L-DD2) has little impact on the abundance pattern, while adopting the other EOS (Q4B5H-SFHo) leads to about a factor of 2 higher and lower abundances for the lightest ($Z \leq 40$) and heaviest ($Z \geq 82$) elements, respectively.
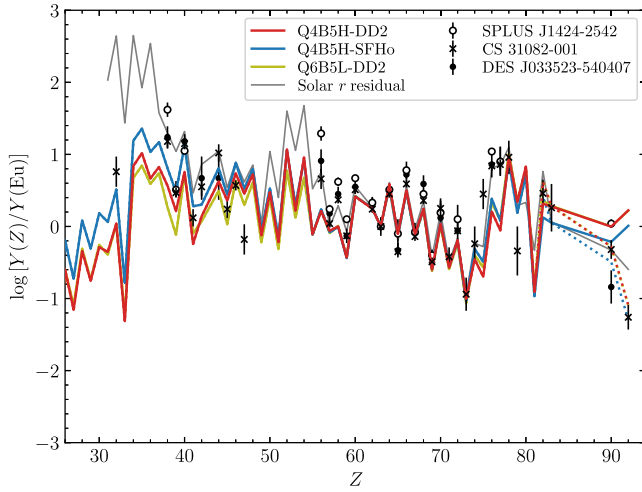
FIG. 3. Elemental abundances normalized by the abundances of Eu for all models. The normalized solar r residuals are also displayed by a gray curve. The dotted lines show the abundances of Pb, Bi, Th, and U at 13 Gyr. The normalized stellar abundances (with error bars) of SPLUS J1424-2542 (open circles), CS 31082-001 (crosses), and DES J033523-540407 (filled circles) are also shown.

Normalized abundances of r-process-enhanced stars SPLUS J1424-2542 [11], CS 31082-001 [36], and DES J033523-540407 [10] are also plotted. These stars exhibit the highest, high (at the criterion for actinide-boost stars in this Letter), and lowest values of measured Th/Eu ratio, respectively. Note that Th and U are α-decaying species (half-lives of 14.05 Gyr, 0.704 Gyr, and 4.47 Gyr for ^{232}Th, ^{235}U, and ^{238}U, respectively), and Pb and Bi are predominantly α-decayed products from long-lived progenitors.

Thus, the abundances of Pb, Bi, Th, and U at 13 Gyr are also shown by dotted lines, given that these stars were born several 100 Myr after the big bang (e.g., Refs. [37–39]). We find that the abundance patterns are in reasonable agreement with those of the stars. In particular, the normalized abundances of Pb, Bi, Th, and U in model Q4B5H-DD2 are in good agreement with those in CS 31082-001, one of the actinide-boost stars.

Actinide boost—Here, we examine the dependencies of actinide production, or Th/Eu, in dynamical ejecta on Y_e and outflow velocity v. The contribution of postmerger ejecta to lanthanide and actinide production is $\sim 0.1\%$–10% (Fig. 2, left), which does not affect our discussion here. The left panel of Fig. 4 shows the abundances of Eu and Th (at 1 yr; all trans-Pb nuclei except for Th and U are assumed to have decayed) as well as the ratio Th/Eu for model Q4B5H-DD2 as functions of Y_e. Here, Y_e is taken to be a free parameter (taking into account possible variation due to the nuclear EOS adopted; see Fig. 5), replacing the original values by a single Y_e. The Eu abundance becomes minimal at $Y_e = 0.175$ as the nuclear flow proceeds toward heavier nuclei. With a reduction of Y_e, Eu becomes abundant owing to fission recycling. The Th abundance reaches a maximum at $Y_e = 0.155$. For $Y_e < 0.155$, we find the effects of "fission waves" for Eu and Th in response to the second and third fission recycling. The multiple fission recycling leads to a convergence of the Th/Eu ratio toward lower Y_e with a few local maxima (for the comparison with the previous study [12], see the Supplemental Material [13]).

Assuming that black-hole–neutron-star mergers are, in part, the sources of r-process elements, we limit the range
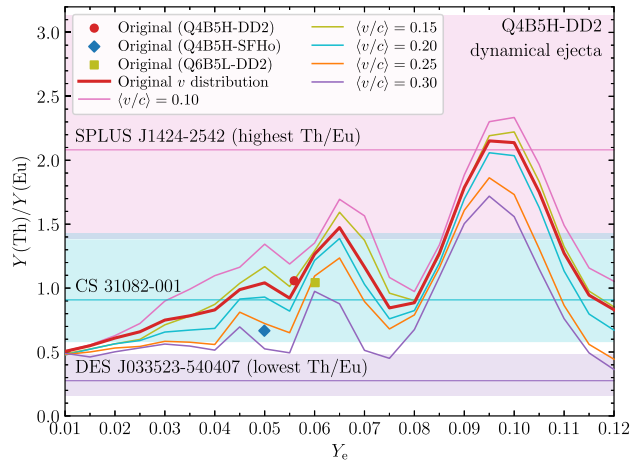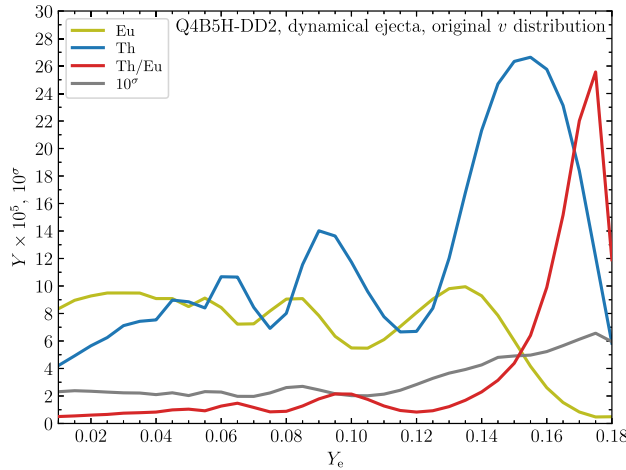

FIG. 4. Abundances of Eu and Th (at 1 yr; all trans-Pb nuclei except for Th and U are assumed to have decayed) as well as the number ratio Th/Eu (in linear scale) for Q4B5H-DD2 (dynamical ejecta) as a function of Y_e (see the text). In the left panel, the factor 10^σ is also shown, which indicates the deviation from the solar r-residual distribution. In the right panel, Th/Eu ratios calculated using tracer particles with given outflow velocities, mass-averaged in the range of ± 0.025, are also shown (labeled as $\langle v/c \rangle$). The symbols indicate the original Th/Eu ratios for Q4B5H-DD2 (circle), Q4B5H-SFHo (diamond), and Q6B5L-DD2 (square) at each mass-averaged Y_e. The horizontal lines (with errors shown by shaded areas) indicate the observational ratios of SPLUS J1424-2542 (magenta), CS 31082-001 (cyan), and DES J033523-540407 (purple), where the abundances of Th are corrected to those of 13 Gyr ago.
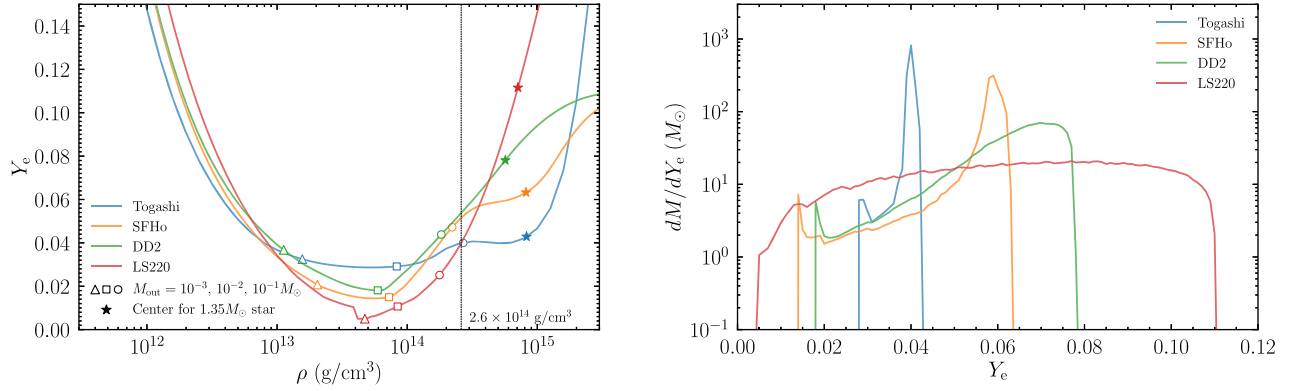
FIG. 5.   Properties of selected EOS (Togashi, SFHo, DD2, and LS220) under the condition of neutrinoless β equilibrium. In the left panel, each curve shows Y_e as a function of matter density ρ with the central value (star) for the $1.35M_\odot$ neutron star. The vertical line indicates the nuclear saturation density. The open triangle, square, and circle symbols mark the masses measured from the surface of the $1.35M_\odot$ neutron star, $M_{out}/M_\odot = 10^{-3}, 10^{-2}$, and 10^{-1}, respectively. The right panel shows the mass distribution of the $1.35M_\odot$ neutron star for each EOS as a function of Y_e.

of Y_e for subsequent discussion. The agreement level of the computed abundances with the solar r residuals can be evaluated by the deviation factor 10^σ with σ defined by $\sigma^2 = \sum_A \left[\log_{10}N(A) - \log_{10}N_\odot(A)\right]^2/n_{tot}$ [2], where $N(A)$ and $N_\odot(A)$ are the normalized isobaric abundances for the dynamical ejecta and the solar r residuals, respectively. The sum runs over the $n_{tot} = 67$ isobars from $A = 139$ to 205, which are predominantly produced in the dynamical ejecta. For Q4B5H-DD2, Q4B5H-SFHo, and Q6B5L-DD2 with original Y_e values, $10^\sigma = 2.2$, 2.1, and 2.0, respectively, indicating agreements with the solar r-residual pattern within about a factor of 2. Here, we regard the abundance patterns with $10^\sigma < 3$ as appropriate models for r-process sources (see also Refs. [2,40]). Thus, hereafter we restrict the range of our attention to $Y_e < 0.12$.

As can be seen in the right panel of Fig. 4, the Th/Eu ratio (the red thick curve; Q4B5H-DD2) reaches the local maxima at $Y_e = 0.050$, 0.065, and 0.095 with an overall decreasing trend toward lower Y_e. The plot also displays the Th/Eu ratios for tracer particles with selected outflow velocities. The symbols indicate the Th/Eu ratios (at mass-averaged Y_e) for all models, which present the levels of actinide boost with original Y_e distributions.

We find substantial variation of the Th/Eu ratio at a given Y_e, with a tendency for this ratio to take on a higher value for a slower ejecta velocity. This is due to the fact that the radioactive heating from r processing heats up the initially cold material up to ~0.7–2 GK (at which so-called $n\gamma$-γn equilibrium, between neutron capture and its inverse, is established [41]). Under this condition, the slower (nearly adiabatically expanding) ejecta achieve higher temperature during an r process. At higher temperature, the r-process path locates closer to β stability (because of $n\gamma$-γn equilibrium), in which β-decay lifetimes are longer. As a result, on the r-process path, more abundances populate in the lighter-mass side ($A < 254$ with few fissile nuclei) than in the

heavier-mass side ($A \geq 254$ with predominantly fissile nuclei) at the end of an r process. The former and the latter include, respectively, the progenitors of Th (by α decay) and Eu (by fission). Thus, the slower ejecta result in a higher Th/Eu ratio, although such a dependency diminishes as Y_e approaches 0.01 because of the multiple fission recycling (that leads to nearly a static nuclear flow).

Higher-Y_e ejecta (with a fixed velocity) also achieve higher temperature because of an initially larger amount of heavy nuclei (^{118}Kr in this Letter; see the Supplemental Material [13]) and thus higher radioactive energy from r processing. Thus, higher-Y_e ejecta tend to result in a higher Th/Eu ratio owing to the r-process path closer to β stability, although the effect of fission waves appears to dominate for $Y_e > 0.05$. It is important to note that the Th/Eu ratio depends in particular on theoretical β-decay predictions [12] (see other nuclear ingredients that affect the actinide production in Refs. [5,12]). The adopted β-decay rates (GT2 [17] based on the HFB-21 mass prediction [18]) appear to result in a relatively high Th/Eu ratio according to Ref. [5].

The stellar Th/Eu ratios of SPLUS J1424-2542 [11], CS 31082-001 [36], and DES J033523-540407 [10] are also presented by horizontal lines in the right panel of Fig. 4, where the observational values of Th are corrected to those 13 Gyr ago (a few Gyr of difference does not substantially change our conclusion). The errors for Th/Eu shown by shaded areas (± 0.18 dex, ± 0.20 dex, and ± 0.24 dex, respectively) are the root mean squares of those for Th and Eu. We find that the models with DD2 result in actinide boost, i.e., Th/Eu > 0.9, which reconcile with the Th/Eu ratio of an actinide-boost star CS 31082-001 but not the highest measured Th/Eu ratio of SPLUS J1424-2542. The model with SFHo does not meet the condition for the actinide boost, although the Th/Eu ratio resides within the range of the error for CS 31082-001.

According to the results with single Y_e values for Q4B5H-DD2 (with the original velocity distribution, red curve), only a range of $Y_e \approx 0.045$–0.070 (or 0.080–0.115, which is unlikely according to available EOS) meets the level of actinide boost, Th/Eu > 0.9, or $Y_e \sim 0.065$ (or 0.085–0.110) for the most actinide-boosted star SPLUS J1424-2542. This result can potentially serve as an important constraint for nuclear EOS, since the dynamical ejecta of black-hole–neutron-star mergers are expected to preserve the original Y_e in the inner crust of neutron stars (for the difference from the case of binary neutron star mergers, see the Supplemental Material [13] and Ref. [30] therein).

The left panel of Fig. 5 displays Y_e as a function of matter density under the condition of neutrinoless β equilibrium for each EOS. Here, two other EOS, LS220 [42] and Togashi [43], are also included (the tables are provided by CompOSE [44–46]; https://compose.obspm .fr). For Togashi, SFHo, LS220, and DD2, the radii (km) of the $1.35M_\odot$ neutron star and maximum masses ($M_\odot$) are (11.6, 2.21), (11.9, 2.06), (12.7, 2.06), and (12.8, 2.42), respectively. For a given EOS, Y_e increases at high density (> several 10^{13} g/cm³) in the presence of symmetry energy. By comparing the curves for DD2 and SFHo with Fig. 1 (top), we find that the matter slightly above the saturation density is tidally ejected (note that the mass below $\sim 10^{13}$ g/cm⁻³ with $Y_e > 0.04$ is subdominant compared to the typical tidal ejecta mass as indicated by open triangles). Given that the matter with a similar density is ejected for other EOS, the possible range in the tidal ejecta is expected to be $Y_e \sim 0.04$–0.06, of which the Togashi EOS does not meet the condition for the actinide boost. As can be seen from the right panel of Fig. 5, the neutron star constructed with the Togashi EOS does not contain the matter with $Y_e > 0.04$, which cannot explain the actinide boost regardless of hydrodynamical conditions.

Conclusion—We have conducted the first exploration of nucleosynthesis based on self-consistent magneto-hydrodynamics simulations of black-hole–neutron-star mergers [31,32]. Lighter ($A < 130$) and heavier ($A > 130$) r-process nuclei were synthesized in the early dynamical and late-time postmerger components, respectively, the ensemble of these reproducing solarlike r-process patterns. This indicates that in addition to binary neutron star mergers, black-hole–neutron-star mergers can also be galactic r-process sites.

Our result has demonstrated that the presence of actinide-boost stars can be explained if the range for the bulk Y_e in the dynamical ejecta of black-hole–neutron-star mergers is $\gtrsim 0.05$ (provided that the trend of Th/Eu for DD2 as a function of Y_e is similar for other EOS). This range of Y_e can be an important constraint on nuclear EOS, such as symmetry energy, under the assumptions that the black-hole–neutron-star mergers are responsible for actinide-boost stars and the matter slightly above the saturation density is tidally ejected. Our result supports a DD2-like EOS, while those without $Y_e \gtrsim 0.05$ components in the neutrons stars are disfavored as to be realistic equations of state, although we should keep in mind potential changes due to uncertainties in relevant nuclear ingredients.

[1] J. J. Cowan, C. Sneden, J. E. Lawler, A. Aprahamian, M. Wiescher, K. Langanke, G. Martínez-Pinedo, and F.-K. Thielemann, Rev. Mod. Phys. **93**, 015002 (2021).

[2] S. Fujibayashi, K. Kiuchi, S. Wanajo, K. Kyutoku, Y. Sekiguchi, and M. Shibata, Astrophys. J. **942**, 39 (2023).

[3] O. Just, A. Bauswein, R. Ardevol Pulpillo, S. Goriely, and H. T. Janka, Mon. Not. R. Astron. Soc. **448**, 541 (2015).

[4] D. Martin, A. Perego, A. Arcones, F. K. Thielemann, O. Korobkin, and S. Rosswog, Astrophys. J. **813**, 2 (2015).

[5] I. Kullmann, S. Goriely, O. Just, A. Bauswein, and H. T. Janka, Mon. Not. R. Astron. Soc. **523**, 2551 (2023).

[6] R. Cayrel, V. Hill, T. C. Beers, B. Barbuy, M. Spite, F. Spite, B. Plez, J. Andersen, P. Bonifacio, P. François, P. Molaro, B. Nordström, and F. Primas, Nature (London) **409**, 691 (2001).

[7] V. Hill, B. Plez, R. Cayrel, T. C. Beers, B. Nordström, J. Andersen, M. Spite, F. Spite, B. Barbuy, P. Bonifacio, E. Depagne, P. François, and F. Primas, Astron. Astrophys. **387**, 560 (2002).

[8] H. Schatz, R. Toenjes, B. Pfeiffer, T. C. Beers, J. J. Cowan, V. Hill, and K.-L. Kratz, Astrophys. J. **579**, 626 (2002).

[9] S. Wanajo, N. Itoh, Y. Ishimaru, S. Nozawa, and T. C. Beers, Astrophys. J. **577**, 853 (2002).

[10] A. P. Ji and A. Frebel, Astrophys. J. **856**, 138 (2018).

[11] V. M. Placco et al., Astrophys. J. **959**, 60 (2023).

[12] E. M. Holmbeck, T. M. Sprouse, M. R. Mumpower, N. Vassh, R. Surman, T. C. Beers, and T. Kawano, Astrophys. J. **870**, 23 (2019).

[13] See Supplemental Material at http://link.aps.org/ supplemental/10.1103/PhysRevLett.133.241201 for more details, which includes Refs. [2,3,5,12,14–30].

[14] R. Abbott et al., Astrophys. J. Lett. **915**, L5 (2021).

[15] S. Wanajo, B. Müller, H.-T. Janka, and A. Heger, Astrophys. J. **852**, 40 (2018).

[16] S. Goriely, S. Hilaire, and A. J. Koning, Astron. Astrophys. **487**, 767 (2008).

[17] T. Tachibana, M. Yamada, and Y. Yoshida, Prog. Theor. Phys. **84**, 641 (1990).

[18] S. Goriely, N. Chamel, and J. M. Pearson, Phys. Rev. C **82**, 035804 (2010).

[19] S. Goriely, M. Samyn, and J. M. Pearson, Phys. Rev. C **75**, 064312 (2007).

[20] K.-H. Schmidt and B. Jurado, Phys. Rev. Lett. **104,** 212501 (2010).

[21] F. X. Timmes and F. D. Swesty, Astrophys. J. Suppl. Ser. **126,** 501 (2000).

[22] K. Hotokezaka, S. Wanajo, M. Tanaka, A. Bamba, Y. Terada, and T. Piran, Mon. Not. R. Astron. Soc. **459,** 35 (2016).

[23] G. Baym, C. Pethick, and P. Sutherland, Astrophys. J. **170,** 299 (1971).

[24] N. Vassh, M. R. Mumpower, G. C. McLaughlin, T. M. Sprouse, and R. Surman, Astrophys. J. **896,** 28 (2020).

[25] S. Goriely, J. L. Sida, J. F. Lemaître, S. Panebianco, N. Dubray, S. Hilaire, A. Bauswein, and H. T. Janka, Phys. Rev. Lett. **111,** 242502 (2013).

[26] S. Goriely, Eur. Phys. J. A **51,** 22 (2015).

[27] N. Vassh, R. Vogt, R. Surman, J. Randrup, T. M. Sprouse, M. R. Mumpower, P. Jaffke, D. Shaw, E. M. Holmbeck, Y. Zhu, and G. C. McLaughlin, J. Phys. G **46,** 065202 (2019).

[28] J. F. Lemaître, S. Goriely, A. Bauswein, and H. T. Janka, Phys. Rev. C **103,** 025806 (2021).

[29] T. Kodama and K. Takahashi, Nucl. Phys. **239,** 489 (1975).

[30] R. Abbott *et al.*, Phys. Rev. X **11,** 021053 (2021).

[31] K. Hayashi, S. Fujibayashi, K. Kiuchi, K. Kyutoku, Y. Sekiguchi, and M. Shibata, Phys. Rev. D **106,** 023008 (2022).

[32] K. Hayashi, K. Kiuchi, K. Kyutoku, Y. Sekiguchi, and M. Shibata, Phys. Rev. D **107,** 123001 (2023).

[33] S. Banik, M. Hempel, and D. Bandyopadhyay, Astrophys. J. Suppl. Ser. **214,** 22 (2014).

[34] A. W. Steiner, M. Hempel, and T. Fischer, Astrophys. J. **774,** 17 (2013).

[35] N. Prantzos, C. Abia, S. Cristallo, M. Limongi, and A. Chieffi, Mon. Not. R. Astron. Soc. **491,** 1832 (2020).

[36] C. Siqueira Mello, M. Spite, B. Barbuy, F. Spite, E. Caffau, V. Hill, S. Wanajo, F. Primas, B. Plez, R. Cayrel, J. Andersen, B. Nordström, C. Sneden, T. C. Beers, P. Bonifacio, P. François, and P. Molaro, Astron. Astrophys. **550,** A122 (2013).

[37] S. Wanajo, Y. Hirai, and N. Prantzos, Mon. Not. R. Astron. Soc. **505,** 5862 (2021).

[38] Y. Hirai, T. C. Beers, M. Chiba, W. Aoki, D. Shank, T. R. Saitoh, T. Okamoto, and J. Makino, Mon. Not. R. Astron. Soc. **517,** 4856 (2022).

[39] J. D. Simon *et al.*, Astrophys. J. **944,** 43 (2023).

[40] S. Goriely, Astron. Astrophys. **342,** 881 (1999), https://ui.adsabs.harvard.edu/abs/1999A%26A...342..881G/abstract.

[41] S. Wanajo, Astrophys. J. Lett. **666,** L77 (2007).

[42] J. M. Lattimer and D. F. Swesty, Nucl. Phys. **A535,** 331 (1991).

[43] H. Togashi, K. Nakazato, Y. Takehara, S. Yamamuro, H. Suzuki, and M. Takano, Nucl. Phys. **961,** 78 (2017).

[44] S. Typel, M. Oertel, and T. Klähn, Phys. Part. Nucl. **46,** 633 (2015).

[45] M. Oertel, M. Hempel, T. Klähn, and S. Typel, Rev. Mod. Phys. **89,** 015007 (2017).

[46] S. Typel, M. Oertel, T. Klähn, D. Chatterjee, V. Dexheimer, C. Ishizuka, M. Mancini, J. Novak, H. Pais, C. Providencia, A. Raduta, M. Servillat, and L. Tolos, arXiv:2203.03209.